Supplementary Material

1. Rainfall Spatial Heterogeneity of $\delta^{18}O$

Discerning the rainfall spatial heterogeneity is an important issue as using the water isotopic tracer for transit time evaluation, particularly in meso-scale catchments. Here, we checked the rainfall spatial heterogeneity of event 2 and event 3 in terms of the rainfall amount and its isotopic composition. The spatial distribution of rainfall amount of each storm was interpolated via inverse distance weighted method (power parameter is 2) by 4 CWB rain gauges (see Fig. 1 in main text). The relative difference (RD) and the coefficient of variation (CV) are calculated for illustrating the spatial heterogeneity (Fig. S1 and Table S1). Note that RD is defined as the rainfall minus the average rainfall of a specific cell divided by the mean rainfall of the entire catchment. In this figure, the CVs of the total rainfall are 16% and 10%, respectively, for event 2 and 3 (Fig. S1(a) and Fig. S1(b)). Such low CVs indicated that the variation were much less than the mean, showing the rainfall spatial pattern is relatively homogeneous. Additionally, the distribution of RD shows that the western part receives more rainfall and the RD has a variation of approx. ±40% of the average. In sum, the both indicator showed that the typhoon-induced rainfall is short-lived, intense, but its rainfall spatial heterogeneity in meso-scale catchments is not pretty large.

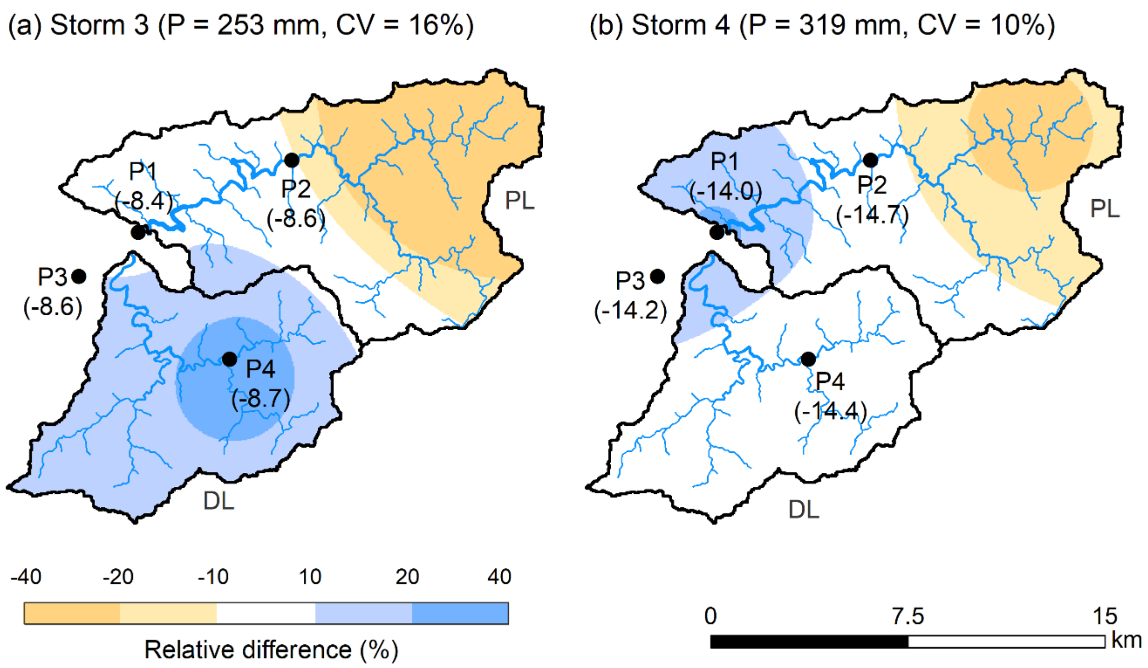

Fig. S1. Rainfall spatial heterogeneity of event 2 (a) and event 3 (b). The black points are rainwater sampling sites with $\delta^{18}O$ value in parentheses.

We further checked the isotopic composition of rainwater during event 2 and 3. The four sampling sites locate in the catchment evenly (Fig. S1). Rain sampling site P1 is close to the streamwater sampling site, so rainwater samples were taken every three hours continuously. On the other hand, we also set three remote sampling sites (P2, P3, and P4) to collect rainwater in bulk for the typhoon period. The isotopic compositions of rainwater are shown in Table S1 and Fig. S1. The differences of $\delta^{18}O$ values between the 4 sites are less than 0.7‰. Theoretically, $\delta^{18}O$ would be gradually depleted with the increase of altitude, whereas the strong convective circulation and torrential rainfall brought by typhoons overwhelms the altitude effect. As a result, the isotopic composition of typhoon rainwater is rather consistent. Our results show a low spatial heterogeneity of rainwater isotopic composition.

Table S1. The altitude, rainfall, and $\delta^{18}O$ at the rainwater sampling sites and for model input.

Gauge ID	Sampling type	Altitude (m)	Event 2		Event 3	
			Rain (mm)	$\delta^{18}O$ (‰)	Rain (mm)	$\delta^{18}O$ (‰)
P1	3-hr	299	335	-8.4	413	-14.0
P2	bulk	327	279	-8.9	333	-14.7
P3	bulk	321	336	-8.6	398	-14.2
P4	bulk	342	378	-8.8	338	-14.4

2. Calibration and Simulation Performance

The best performance measures, KGE and the three perspectives of streamflow and $\delta^{18}O$ simulations are listed in Table S2. The streamflow simulations are satisfactory for all catchment-events. All KGE_Q for the two catchments are higher than 0.85; the correlation (*r*) ranges from 0.87 to 0.97; the variability ratio (*V*) ranges from 0.93 to 1.06, and the bias error (*B*) ranges from 0.94 to 1.04. The KGE_C simulations are also satisfactory ranging from 0.96 to 0.99 and 0.75 to 0.90 for PL and DL, respectively with PL better than DL. Note that event 5 in both catchments could not be simulated promisingly. Specifically, the individual performance of the three perspectives of KGE are at the similar level in the two catchments for $\delta^{18}O$ simulation.

Table S2. Best performance for simulating streamflow and $\delta^{18}O$. KGE and *V*, *B*, and r represent the Kling–Gupta efficiency coefficient, variability ratio, bias error, and correlation, respectively.

Catchment-Event	Streamflow				$\delta^{18}O$			
	KGE_Q	*V*	*B*	r	KGE_C	*V*	*B*	r
PL01	0.924	0.993	0.975	0.928	0.966	0.999	1.001	0.966
PL02	0.944	0.976	0.984	0.952	0.993	1.001	1.001	0.993
PL03	0.921	1.057	1.039	0.962	0.964	0.998	1.001	0.965
PL04	0.937	1.035	1.000	0.947	0.978	1.000	1.001	0.978
PL05	0.938	0.965	0.983	0.952	0.608	0.998	1.012	0.608
PL06	0.966	0.990	0.992	0.969	0.983	1.002	0.998	0.983
DL01	0.885	0.954	0.935	0.917	0.900	0.931	0.996	0.929
DL02	0.934	0.995	0.951	0.956	0.846	1.053	1.023	0.858
DL03	0.851	0.926	1.025	0.873	0.749	1.139	1.020	0.792
DL04	0.903	0.947	0.986	0.920	0.826	0.885	0.999	0.870
DL05	0.933	0.975	0.978	0.941	0.731	0.943	0.989	0.737
DL06	0.953	1.021	0.965	0.975	0.882	0.919	0.969	0.920

3. Complied TRANSEP model results

We reviewed and summarized 55 events of 6 cases which used TRANSEP model to estimate MTT_{ew} and F_{ew} in different environments. Notably, all drainage areas are less than 8.8 km^2, lacking of meso-scale catchments. Rainfall amount in most cases are less than 70 mm, which is much smaller than our events (236 mm), except one event in WS10, Oregon (177 mm). As for duration of storm, most cases are shorter than one day except for one case in Oregon which is comparable to our typhoons that usually last for two to three days. All rainfall intensity is similar to our cases. $\delta^{18}O$ are used as tracer except in Johnson et al. (2007) who used dissolved CO_2. The MTT_{ew} and F_{ew} range from 1.0 to 93.8 h and 0.04 to 0.77, respectively.

Table S3. Complied TRANSEP model studies at a storm-scale.

Site	Lati-tude	Area (km^2)	Tracer	Rainfall (mm)	Duration (h)	I (mm/h)	Q/P	Transfer Function	MTT_{ew}	F_{ew}	Reference
K, Maimai, New Zeland	42	0.17	^{18}O	27	13.0	2.1	0.19	EPM	10.5	0.22	Weiler et al. (2003)
				70	30.0	2.3	0.52	TPLR	10.0	0.18	
Juruena, Mato Grosso, Brazil	10.5	0.02	Dissolved CO_2	30.7	0.5	61.4	0.05	TPLR	-	0.17	Johnson et al. (2007)
				20	0.8	26.7	0.04			0.1	
				16.8	1.8	9.6	0.03			0.32	
				5	1.3	3.8	0.03			0.08	
				3.6	0.3	14.4	0.04			0.15	
				27.8	2.3	12.4	0.06			0.48	
				2.4	0.4	5.8	0.02			0.05	
				10.7	0.6	18.3	0.04			0.30	
				6.1	2.0	3.1	0.04			0.14	
				14.6	0.8	19.5	0.04			0.26	
				3	0.8	4.0	0.04			0.04	
				11.1	0.8	13.3	0.05			0.26	
				15.7	1.3	12.6	0.06			0.27	
				14.5	0.4	34.8	0.06			0.25	
Upper Sabino, AZ	32	8.8	^{18}O	26	3.0	8.7	0.72	EM	4.5	0.23	Lyon et al. (2008)
Hillslope, HJ Andrews, Oregon	44	0.002	^{18}O	31	61.8	0.5	0.04	GM	15.0	0.22	McGuire and McDonnell (2010)
				60	82.5	0.7	0.23	TPLR	14.0	0.06	
WS10, HJ Andrews, Oregon	44	0.102		177	107.5	1.6	0.03	TPLR	28.0	0.11	
				31	61.8	0.5	0.07	GM	8.0	0.27	
				60	82.5	0.7	0.21	TPLR	34.0	0.10	
B1, Columbia	5	1.59	^{18}O	24	4.5	5.3	0.10	TPLR	26.1	0.23	Roa-Garc´ıa and Weiler (2010)
				38	4.8	8.0	0.11		1.5	0.24	

				30	2.8	10.9	0.05		25.7	0.32	
B2, Columbia	5	1.8		24	4.5	5.3	0.21		50.8	0.25	
				24	4.8	5.1	0.14		6.8	0.40	
				31	4.0	7.8	0.28		66.7	0.21	
BB, Columbia	5	0.62		16	3.3	4.9	0.25		3.3	0.12	
				21	3.8	5.6	0.36		5.3	0.27	
				16	3.8	4.3	0.19		14.4	0.14	
SB, Canada	46	0.07	^{18}O	14.1	1.2	11.8	-	TPLR	7.6	0.33	Segura et al. (2012)
AW, Canada	46	0.11		25.2	10.3	2.4	-		1.2	0.77	
				14.1	1.2	11.8	-		11.9	0.29	
				38.1	2.4	15.9	-		1.7	0.52	
				7	2.9	2.4	-		4.4	0.28	
VC, Canada	46	0.11		14.1	1.2	11.8	-		1.5	0.55	
				38.1	2.4	15.9	-		1.0	0.42	
YV, Canada	46	0.3		25.2	10.3	2.4	-		33.4	0.32	
				14.1	1.2	11.8	-		31.3	0.42	
SC, Canada	46	0.38		25.2	10.3	2.4	-		16.1	0.31	
				14.1	1.2	11.8	-		1.2	0.36	
				38.1	2.4	15.9	-		12.9	0.52	
				7	2.9	2.4	-		7.0	0.40	
PW, Canada	46	0.48		14.1	1.2	11.8	-		26.6	0.34	
				38.1	2.4	15.9	-		1.1	0.60	
				7	2.9	2.4	-		26.3	0.19	
EF, Canada	46	0.91		14.1	1.2	11.8	-		3.1	0.30	
				38.1	2.4	15.9	-		31.4	0.47	
				7	2.9	2.4	-		12.0	0.21	
LK, Canada	46	1.47		25.2	10.3	2.4	-		93.8	0.51	
				14.1	1.2	11.8	-		11.7	0.33	
				38.1	2.4	15.9	-		4.7	0.52	
				7	2.9	2.4	-		60.3	0.23	

4. Correlation between hydrometrics and model parameters

Correlation analysis reveals significant correlations between hydrometrics and the best-fit model parameters (Table S4). In the streamflow module, parameter a_1 and a_3 in loss function are negatively correlated to intensity-related hydrometrics, i.e., I, P_{max3hr} and Q_{max}. Parameter α_q is negatively correlated to P, P_{max3hr} and Q_{max}, but not correlated to rainfall intensity. In the tracer module, both parameters in loss function are not correlated to hydrometrics. Shape parameter in event water transfer function (α_e) is negatively correlated to intensity-related hydrometrics (I, P_{max3hr} and Q_{max}). No significant correlation between F_{ew} and all hydrometrics are found; however, MTT_{ew} is negatively correlated to I and P_{max3hr}. In sum, the intensity-related hydrometrics (I and P_{max3hr}) are major controls on the both streamflow and tracer modules.

Table S4. Pearson correlation coefficients between logarithmic hydrometric characteristics and logarithmic parameters for the storms. Values underlined and in bold are statistically significant with 95% and 99% level of confidence ($p< 0.05$ and $p<0.01$), respectively.

Parameter	P	D	I	P_{max3hr}	Q	Q_{max}	AP_{7day}
a_1	-0.38	0.07	<u>-0.61</u>	**-0.76**	-0.23	**-0.70**	0.05
a_2	0.10	-0.03	0.17	0.35	0.05	0.33	-0.04
a_3	-0.20	0.22	<u>-0.56</u>	<u>-0.66</u>	-0.06	<u>-0.56</u>	0.19
α_q	**-0.70**	-0.47	-0.37	**-0.78**	<u>-0.63</u>	**-0.75**	-0.40
β_q	0.17	**0.70**	<u>-0.66</u>	-0.29	0.30	-0.24	**0.70**
b_1	-0.44	-0.45	-0.04	-0.49	-0.28	-0.44	-0.45
b_2	0.27	0.23	0.09	0.47	0.10	0.36	0.38
α_e	-0.51	0.00	**-0.71**	**-0.79**	-0.37	**-0.76**	0.02
β_e	0.33	0.22	0.17	0.36	0.30	0.36	0.21
MTT_{ew}	-0.22	0.29	**-0.68**	<u>-0.54</u>	-0.07	-0.49	0.30
F_{ew}	0.08	-0.32	0.52	0.28	0.14	0.29	-0.23

5. Time-variant sensitivity analysis

Time-variant sensitivity analysis is used to imply the dynamics of rainfall-runoff generation in models. The parameter sensitiveness was generalized from 12-h moving windows Morris's μ into three segments. The Morris's μ are divided into three segments; they are rising, peak, and recession segments in accordance with hydrograph. The rising segment (seg. 1) is from streamflow risng to the peak flow; the peak segment (seg. 2) is from peak to the inflection point of the recession; the recession segment (seg. 3) indicates the streamflow from the inflection to the end of the rainstorm. The Morris's μ in each segment is then averaged. Results of the three most sensitive parameter α_e, α_q and b_1 are listed in Table S5. Compared among the three parameters, α_q and b_1 have a similar pattern, in which the μ values ranking from high to low are seg. 2, seg. 3 and seg. 1. On the other hand, the μ value of α_e ranks from seg. 2, seg. 1 to seg. 3 in descending sequence. The storm magnitude does not have a significant effect on the μ values of the three parameters. Intriguingly, the highest μ value of α_e appears in seg. 1 during the small rainstorms (event 2, 4 and 5) in DL. In sum, the both shape parameters (α_q, α_e) play a predominant role in generating the quick flow, whereas parameter, b_1, gets important during recession indicating rainfall partitioning regulates the runoff generation after peak flow. Obviously, the sensitiveness of parameters varies with different segments, implying the necessity of time-variant parameterization.

Table S5. Morris's μ value of the sensitive parameters in the three segments of hydrograph in the catchment-events.

Catchment Event	α_e			α_q			b_1		
	seg. 1	seg. 2	seg. 3	seg. 1	seg. 2	seg. 3	seg. 1	seg. 2	seg. 3
PL01	15.2	32.2	5.8	5.8	25.6	21.9	8.6	16.9	38.2
PL02	31.8	68.3	20.1	44.2	172.7	101.1	5.1	20.3	28.7
PL03	39.8	65.1	8.3	8.1	47.4	35.1	12.4	31.7	61.5
PL04	18.1	14.4	6.1	6.6	20.5	19.9	11.8	20.8	29.3
PL05	4.7	13.3	1.1	1.2	3.5	3.9	3.7	4.5	9.3
PL06	158.2	172.1	7.8	94.2	205.1	55.1	14.4	24.6	23.9
DL01	12.0	17.6	4.0	3.5	14.6	14.3	12.3	14.5	30.1
DL02	44.1	37.5	5.0	38.6	83.2	36.8	2.9	14.5	25.3
DL03	29.6	42.4	8.6	9.8	46.1	35.6	15.9	25.8	54.0
DL04	34.5	13.0	6.4	9.3	26.6	23.8	11.2	18.7	29.3
DL05	21.5	13.1	1.2	9.4	16.1	7.3	14.7	15.9	14.9
DL06	128.5	148.1	3.8	68.7	164.2	38.6	10.8	20.2	20.4